Supplementary Information for

Real-time tracking of single-molecule collagenase on the native collagen and partially-structured collagen-mimic substrates

James Froberg, Woo-Sik Choi, Abbas Sedigh, Tayebeh Anajafi, Jasmin Farmakes, Zhongyu Yang, Sanku Mallik, D. K. Srivastava, and Yongki Choi*

Departments of Physics, Chemistry and Biochemistry, and Pharmaceutical Science, North Dakota State University, Fargo, ND 58108, United States

Table of Contents

1. Materials

Lipopeptides ($[CH_3(CH_2)_{16}CONH$-GPQGIAGQR$(GPO)_2$GG; O represents 4-(*R*)-hydroxyproline] (6 μM) and Pyrene-IDA-Cu^{2+} were synthesized using previously published protocols.[1-4] Collagen type I (rat tail, 1 mg/ml, Corning) was diluted to 1 - 100 μg/ml in either PBS buffer or an assay buffer (100 mM Tris-HCl, pH 7.5, containing 100 mM NaCl, 10 mM $CaCl_2$) for each measurement. All other chemicals were purchased commercially from Ezno life sciences, Biomol laboratories, Acros Organics, EMD, Fisher Scientific, or Sigma Aldrich. All regents were used as received without further purification.

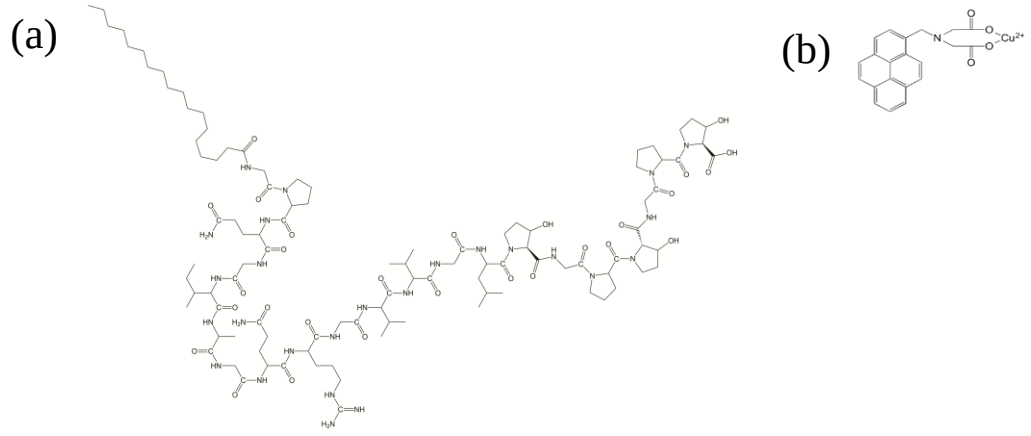

Figure S1. Chemical structures of (a) a lipopeptide and (b) a pyrene-IDA-Cu^{2+} linker.

2. CD Spectroscopy Measurements

All of the CD spectra were performed in 10 mM phosphate buffer (pH = 7.4) at various temperatures. The spectra were measured in the continuous scanning mode (λ = 270 - 180 nm) with a data pitch of 0.2 nm and a scan speed of 100 nm/min. Figure S2 showed no positive values at λ = 220 - 225 nm over the wide range of temperatures from 5 °C to 60 °C, which is a characteristic of triple-helical conformation,[5] suggesting no triple helicity for the lipopeptides.

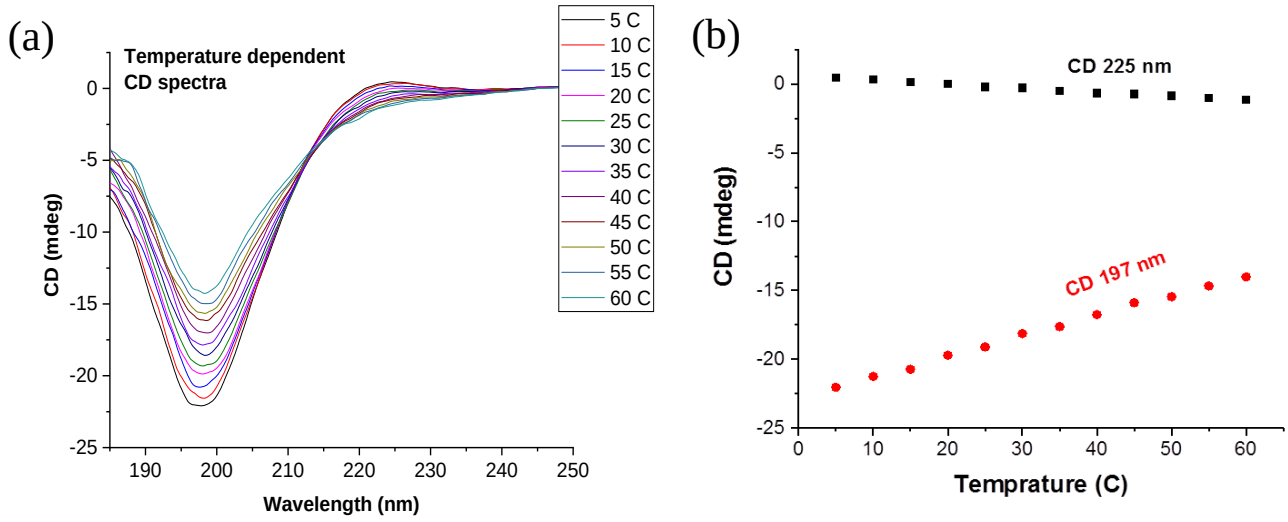

Figure S2. (a) Temperature-dependent CD spectra of lipopeptides. (b) Temperature-dependent maximum-positive and minimum-negative CD values at λ = 197 nm and λ = 225 nm, receptively.

3. Atomic force microscopy measurements

The imaging measurements were performed using a commercial atomic force microscope (NT-MDT NTEGRA AFM). All samples were imaged either under ambient conditions in a semi-contact mode with a resonant frequency of 190 kHz silicon AFM probes (Budget sensors) or liquid conditions in a semi-contact/contact mode with a resonant frequency of 1 - 10 kHz soft silicon nitride AFM probes (Nano World). The samples were prepared by 10 - 50 µl of each solution on Mica/silicon surface for 5 - 30 min in a sealed compartment to protect from evaporation at either room temperature or 4 °C. For air imaging, the samples were washed with deionized water (Millipore) repeatedly, and dried under purified nitrogen flow. For liquid imaging, the samples were directly imaged in the buffer without drying and perfused by 1 - 10 µl of MMP1 solution. The images were flattened to eliminate the background low-frequency noise and tilt from the surface using all unmasked portions of scan lines to calculate individual least-square fit polynomials for each line.

4. Cloning, expression, purifications, and enzymatic assay of MMP1

The plasmid containing the coding sequence of MMP1 (pCMB6-XL6, SC118645) was purchased from OriGene Technologies Inc., Rockville, MD. The DNA sequence of the catalytic

domain of MMP1 was amplified by PCR using the forward and reverse primers being 5′-CCAGGGAGCAGCCTCGTTTGTCCTCACTGAGGGGAAC-3′ and 5′-GCAAAGCACCGGCCTCGTTATTTGGACTCACACCATGTGTTTTCCA-3′, respectively. The PCR amplicon was cloned in in the LIC vector (obtained from Dr. Bottomley's lab).[6, 7] The resultant plasmid was transformed in *E. coli* BL21 (DE3) cells, and the enzyme was expressed by growing the cells in LB Media containing 1 mM IPTG at 37 °C for 5 hrs. The cells were harvested by centrifugation at 8000 g for 20 min, sonicated 10 min on ice (Buffer A: 50 mM Tris-HCl, pH 7.5 containing 1 mM PMSF), and the pellets were separated by centrifugation at 15000 rpm for 30 min. All the expressed MMP1 was found to be present in the inclusion bodies, from which the active enzyme was obtained by washing the pellet by urea followed by the serial dilution as described previously.[8] First, the cell pellets were washed three times by buffer A containing 2 M urea, and then they were dissolved in buffer A containing 6 M urea by stirring overnight at 4 °C. The urea solubilized MMP1 was subjected to a serial dilution against decreasing concentrations of urea in buffer B (50 mM Tris-HCl, pH 7.5 containing 10 mM $CaCl_2$ and 10 µM $ZnCl_2$). The above treatment resulted in the refolding of MMP1 with restoration of catalytic activity. The refolded protein was found to be nearly homogeneous by SDS-PAGE.

The enzymatic assay of MMP1 were performed on a fluorescence microplate reader in the assay buffer (100 mM Tris-HCl, pH 7.5, containing 100 mM NaCl, 10 mM $CaCl_2$) containing 5 µM MMP/TACE FS-6 substrate and appropriately diluted purified form of MMP1. The cleavage of the substrate resulted in an increase in the fluorescence at 400 nm (λ_{ex} = 325 nm) which was recorded as a function of time. A representation trace for the time course of the MMP1 catalyzed cleavage of the substrate is shown in Figure S3.

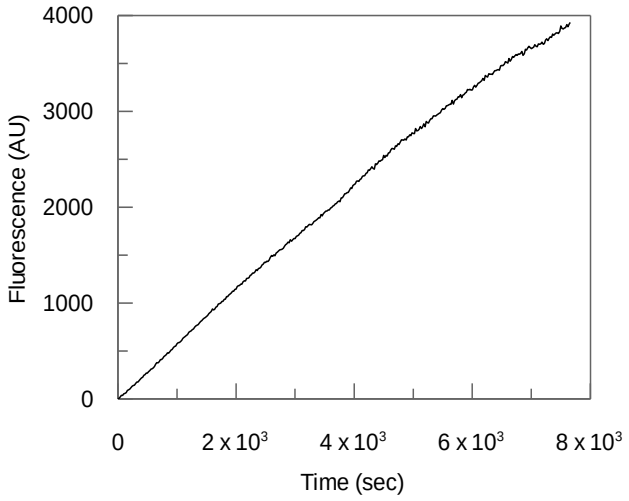

Figure S3. A representative trace of MMP1 catalyzed reaction for the cleavage of 5 µM MMP/TACE FS-6 substrate by 5 nM enzyme in the assay buffer. The increase in fluorescence (arbitrary unit, AU) at 400 nm (λ_{ex} = 325 nm) as a function of time is shown. The thick solid straight line is shown to denote the linear range of the catalytic reaction.

5. Nano-circuit device fabrication and measurements

SWNTs were grown by chemical vapor deposition (CVD), followed by optical lithography for patterning electrodes and electron beam lithography for the electrodes passivation described previously.[9, 10] Devices were functionalized using a bifunctional linker molecule, pyrene-IDA-Cu^{2+}. The pyrene functionality adheres to the SWNT sidewall strongly via π-π stacking.[11] A solution of the linker molecules in ethanol (1 mM) was prepared. Devices were soaked in solution for 15 min without agitation, and then washed with 0.1% Tween-20 (Acros Organics) in ethanol to remove excess linker molecules. Then, the devices were rinsed under flowing de-ionized water. The devices were soaked in the MMP1 solution (6 μM) for 20 min without agitation. Next, the devices were washed with the buffer thoroughly to remove unattached MMP1. Following conjugation, devices were stored in the buffer solution and neither dried nor imaged until the completion of measurements. Figure S4 depicts an example of the single-molecule nanocircuit.

All electronic measurements were performed with the active portion of the device submerged in the buffer solution. The potential of the electrolyte was controlled using Pt counter and pseudo-reference electrodes, and held at 0 ~ -0.4 V vs. Pt using Keithley 2400 sourcemeter. The source-drain bias was held at 0.1 V. A Keithley 428 preamplifier operating at 10^8 V/A gain and with a 40 μs rise time was used to measure the source-drain current of the device. Data was collected for at least 600 s for each measurement condition. The analysis has been performed using a 10-Hz, digital low pass filter to $\Delta I(t)$ from $I(t)$.[10]

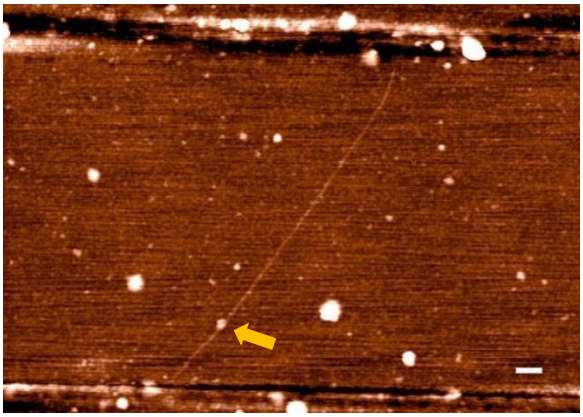

Figure S4. Example AFM topography of SWNT-FET device with a single MMP attachment (arrow). Scale bar is 200 nm.

6. Signal transduction mechanisms

The SWNT-FET is extremely sensitive to electrostatic gating by the protein's charged residues within few nm of the attachment site.[12] When a protein undergoes its conformational rearrangement, the movement of these charges generates a time-varying electric fields that acts in addition to the constant, externally applied gating voltage V_G to produce a time-varying

change in gating ΔV_G. Considering a set of protein charges q_i dynamically varying between positions $r_{i,1}$ and $r_{i,2}$, the consequence of these charges on the SWNT current will be,

$$\Delta I = \frac{\partial I}{\partial V_G}\Delta V_G \propto \frac{\partial I}{\partial V_G}\sum_i q_i\left(\frac{1}{r_{i,1}} - \frac{1}{r_{i,2}}\right)\exp(-r_{i,1}/\lambda_D)$$

where λ_D is the Debye screening length of the electrolyte. In this equation, the variability of $\Delta I(t)$ from one device to another is entirely due to the slope $\partial I/\partial V_G$, which is an empirical, device-dependent parameter. Otherwise, the q_i and r_i terms in the above equation are entirely determined by enzyme's structure and movements.[12]

Figure S5 illustrates the schematic diagram of the MMP1-SWNT interface, showing the close-up X-ray structures of MMP1 in its closed and open conformations (PDB: 1HFC and 3SHI).[13, 14] There is uncertainty in the orientation of the MMP1 at the SWNT, since the orientation of the pyrene linkers and MMP1 are not easily defined. Nevertheless, we have selected an energetically likely orientation of the pyrene-IDA linkage in its rotational orientation that allows binding to the N-terminal in one of two possible rotomers.[15] With this model, the high current state could result from two charge residues around the N-terminal; a positively charged Arg198 residue moves away from the SWNT and a negative charged Glu110 residue moves close to the SWNT during the conformational changes. In this model, the fields can be calculated under the pyrene rings, where perturbation of the SWNT should lead to the most sensitive interactions, and compared to the gating ΔV_G observed experimentally to further support the orientation of MMP1 with respect to the SWNT.[12] More detailed analysis requires precise knowledge of the pyrene linker's orientation and the SWNT's response to the fields, both of which are formidable characterization challenges. It should be noted that that the two residues are most likely responsible for signal generation, there could be additional contribution from other charged residues within few nm of the attachment site.

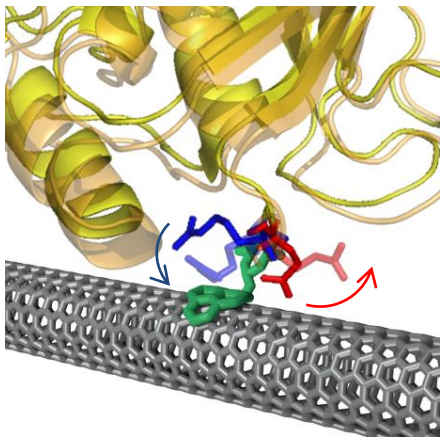

Figure. S5. Detailed view of the MMP1-SWNT interface, showing crystal structures of the MMP1 in its closed and open conformations.

7. References

1. J. Banerjee, A. J. Hanson, B. Gadam, A. I. Elegbede, S. Tobwala, B. Ganguly, A. V. Wagh, W. W. Muhonen, B. Law, J. B. Shabb, D. K. Srivastava and S. Mallik, *Bioconjugate Chemistry*, 2009, **20**, 1332-1339.
2. N. Sarkar, J. Banerjee, A. J. Hanson, A. I. Elegbede, T. Rosendahl, A. B. Krueger, A. L. Banerjee, S. Tobwala, R. Wang, X. Lu, S. Mallik and D. K. Srivastava, *Bioconjugate Chemistry*, 2008, **19**, 57-64.
3. J. Banerjee, A. J. Hanson, E. K. Nyren-Erickson, B. Ganguli, A. Wagh, W. W. Muhonen, B. Law, J. B. Shabb, D. K. Srivastava and S. Mallik, *Chemical Communications*, 2010, **46**, 3209-3211.
4. A. I. Elegbede, J. Banerjee, A. J. Hanson, S. Tobwala, B. Ganguli, R. Wang, X. Lu, D. K. Srivastava and S. Mallik, *J. Am. Chem. Soc.*, 2008, **130**, 10633-10642.
5. G. Melacini, Y. Feng and M. Goodman, *J. Am. Chem. Soc.*, 1996, **118**, 10359-10364.
6. R. K. Singh, T. Mandal, N. Balasubramanian, G. Cook and D. K. Srivastava, *Analytical Biochemistry*, 2011, **408**, 309-315.
7. L. D. Cabrita, W. Dai and S. P. Bottomley, *BMC Biotechnology*, 2006, **6**, 12-12.
8. S. Tobwala and D. K. Srivastava, *Adv. Enz. Res.*, 2013, **1**, 17-29.
9. B. R. Goldsmith, J. G. Coroneus, V. R. Khalap, A. A. Kane, G. A. Weiss and P. G. Collins, *Science*, 2007, **315**, 77-81.
10. Y. Choi, I. S. Moody, P. C. Sims, S. R. Hunt, B. L. Corso, G. A. Weiss and P. G. Collins, *Science*, 2012, **335**, 319-324
11. R. J. Chen, Y. Zhang, D. Wang and H. Dai, *J. Am. Chem. Soc.*, 2001, **123**, 3838-3839.
12. Y. Choi, T. J. Olsen, P. C. Sims, I. S. Moody, B. L. Corso, M. N. Dang, G. A. Weiss and P. G. Collins, *Nano Lett.*, 2013, **13**, 625-631.
13. J. C. Spurlino, A. M. Smallwood, D. D. Carlton, T. M. Banks, K. J. Vavra, J. S. Johnson, E. R. Cook, J. Falvo, R. C. Wahl, T. A. Pulvino and et al., *Proteins*, 1994, **19**, 98-109.
14. I. Bertini, V. Calderone, L. Cerofolini, M. Fragai, C. F. Geraldes, P. Hermann, C. Luchinat, G. Parigi and J. M. Teixeira, *FEBS Lett*, 2012, **586**, 557-567.
15. H. Schrauber, F. Eisenhaber and P. Argos, *J. Mol. Biol.*, 1993, **230**, 592-612.